PNAS RESEARCH ARTICLE | APPLIED PHYSICAL SCIENCES

Collapsible scissored surfaces

Noah Toyonaga[a], Seri Nishimoto[b], Colter J. Decker[c], Robert J. Wood[c], Tomohiro Tachi[b,d], and L. Mahadevan[a,c,e,1]

Edited by John A. Rogers, Northwestern University, Evanston, IL; received February 21, 2026; accepted March 30, 2026

We introduce an additive approach for the design of a class of transformable structures based on two-bar linkages ("scissor mechanisms") joined at vertices to form a two-dimensional mesh which we call a pantograph lattice. Our approach shows how these lattices unfold from a one-dimensional collapsed state to two-dimensional surfaces of single and double curvature. We provide an algorithm for growing pantograph structures that allows us to explore the full space of possible mechanisms, and we use it to computationally design and physically assemble a series of examples of varying complexity. We finally demonstrate a streamlined method for automated fabrication of pantograph lattices using multimaterial 3D printing.

geometric metamaterial | linkage | mechanism | origami

Discrete mechanical metamaterials—structures assembled from simple kinematic elements such as folds, cuts, and hinges—provide a versatile way to program complex shape change. Origami and kirigami systems (1–7) exemplify this idea: aggregating basic units like creases or slits yields deployable surfaces with rich but analytically tractable geometric behavior. These discrete approaches have enabled a broad class of transformable architectures whose motions and final configurations can be understood and designed through local geometric rules.

A parallel tradition uses linkages rather than folds or cuts as the fundamental building blocks. Among these, the two-bar linkage, or scissor mechanism, appears widely across natural and engineered systems: from the nanometer-scale contractile injection machinery of bacteriocidal viruses (8), to pantographic drawing tools, extendable electrical connectors on trains and buses, bathroom mirror extenders, and deployable space structures (9). A scissor linkage is an elementary kinematic mechanism consisting of two rigid bars joined by a pivot (Fig. 1*A*); multiple scissors can be joined into 1D chains (for a more technical discussion, see below) (10) in which each scissor is connected only to two neighbors—for example in a bathroom mirror (Fig. 1*C*). Variations with different linkage lengths (or bent linkages) enable 1D chains to deploy to various plane curves or form closed loops (11). The Hoberman sphere is a well-known variation, and can be interpreted as a set of interlinked 1D scissor chains (11, 12). Such mechanisms typically form one-dimensional chains that extend or contract linearly, and they invite a natural question: can the logic of scissor-based mechanisms be extended to two dimensions to approximate general surfaces, much as origami extends planar crease patterns into 3D shapes?

Here we consider 2D lattices ("pantograph lattices") in which discrete scissors are connected along four distinct sides (Fig. 1*E*). Recent studies have explored aspects of this question, e.g., using an optimization approach to design scissor lattices that deploy from a planar configuration (13), or considering fully collapsible chebyshev net-like networks of elastic strips (14). These efforts demonstrate the potential of linkage-based metamaterials to achieve nontrivial morphologies. Pantograph lattices also bear some similarities to elastic gridshells (15–20), which are deployable structures made of long, elastic beams joined to an arbitrary number of neighbors. However, in a pantograph lattice, beams are the length of a single unit cell (a scissor) and are thus joined only to immediate neighbors. Additionally, gridshell structures typically rely on the bending of structural members to achieve their three-dimensional conformation; in contrast, pantograph lattices can achieve a diversity of morphologies from purely geometric considerations. Thus, while gridshell design typically requires global energetic optimization that scales with system size (9, 16–19), pantograph lattices offer a purely geometric route to controlling shape by reducing global geometry and kinematics to a series of local, analytically soluble algebraic constraints, which enables our closed form, additive approach to design.

The present work complements these studies by providing an analytical exploration of the design space for two-dimensional assemblies of rigid scissor linkages joined by planar joints at the ends (Fig. 1). Our main result is a method to design pantograph lattices with arbitrary leg lengths which are 1) reconfigurable with a single kinematic degree

Significance

The two-bar linkage, or scissor mechanism, is an elementary machine which can close to a one-dimensional state in which both legs are parallel. We describe a class of geometric metamaterials based on lattices of scissor mechanisms which transform from a one-dimensional collapsed state to map two-dimensional surfaces. We derive an analytic "additive" algorithm which parameterizes the space of all such structures, paving the way for us to design metastructures with programmable form and function.

Author affiliations: [a]Department of Physics, Harvard University, Cambridge, MA 02138; [b]Department of Architecture, The University of Tokyo, Tokyo 101-0003, Japan; [c]School of Engineering and Applied Sciences, Harvard University, Cambridge, MA 02138; [d]Graduate School of Arts and Sciences, The University of Tokyo, Tokyo 153-0041, Japan; and [e]Department of Organismic and Evolutionary Biology, Harvard University, Cambridge, MA 02138

Author contributions: N.T. and L.M. conceived research; N.T., R.J.W., T.T., and L.M. designed research; N.T., S.N., and C.J.D. performed research; N.T. analyzed data; and N.T., S.N., C.J.D., R.J.W., T.T., and L.M. wrote the paper.

The authors declare no competing interest.

This article is a PNAS Direct Submission.

[1]To whom correspondence may be addressed. Email: lmahadev@g.harvard.edu.

This article contains supporting information online at https://www.pnas.org/lookup/suppl/doi:10.1073/pnas.2605221123/-/DCSupplemental.

Published June 18, 2026.

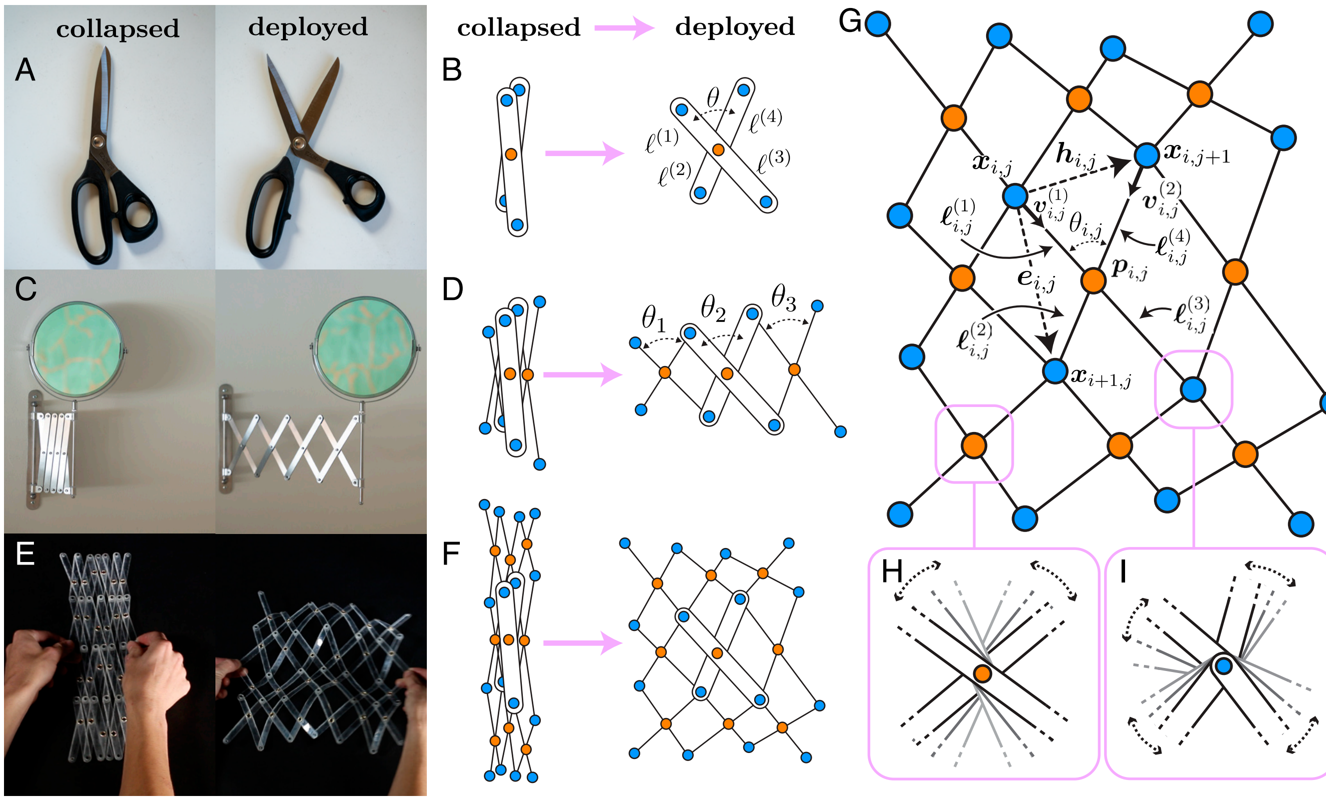

Fig. 1. Geometry and kinematics. (*A*) A pair of handheld scissors is the prototypical example of a two bar linkage, the atomic mechanism of pantograph systems. (*B*) A single scissor mechanism can be characterized by four leg lengths and an opening angle. (*C* and *D*) The mount for a bathroom mirror is an example of a one-dimensional chain of identical scissor mechanisms (a pantograph). Here the coupling of opening angles (θ_1, θ_2, θ_3) allows for the telescopic extension of the mirror from the wall. (*E* and *F*) Using the methods developed in this paper we can design collapsible, two-dimensional lattices of scissors, which we name pantograph lattices. As an example we show a doubly curved "eggbox," which is further described in **additive construction**. (*G*) Notation used to describe a pantograph lattice. A single scissor ($\boldsymbol{S}$) is composed of two rods (represented by black lines) joined by a scissor pivot (orange circle). Multiple scissors can be joined together using vertex pivots (blue). The geometry of a scissor can be fully described by the combination of two leg direction vectors ($\{\boldsymbol{v}^{(1)}, \boldsymbol{v}^{(2)}\}$) and four leg lengths ($\{\ell^{(1)} \ldots \ell^{(4)}\}$). For convenience we also introduce the edge vectors, $\boldsymbol{e}$ and $\boldsymbol{h}$ which connect the tips of the upper and left legs, respectively. (*H*) Scissor pivots (orange) join the legs of a single scissor and enforce coplanarity while (*I*) vertex pivots (blue) connect 4 scissors and allow for independent orientation of each leg (including out-of-plane).

of freedom (deployable), 2) collapse to a configuration in which all linkages are parallel (collapsible) and 3) have a deployed configuration in which all scissor legs are straight (rigid-embeddable). We show analytically that an $M \times N$ pantograph lattice satisfying these criteria is described by $M+N$ independent design parameters, and we develop an additive construction procedure that generates all such deployable, collapsible lattices. This approach unifies and extends prior work by characterizing the full intrinsic design space of scissor lattices that collapse to a one-dimensional configuration (similar to that treated in ref. 14) while allowing arbitrary leg lengths (as in ref. 13). We further validate the construction with computational design tools and physical prototypes fabricated by additive manufacturing.

Mathematical Framework

We now provide a formal definition of the notation used throughout our work. A scissor (denoted $\boldsymbol{S}$) is parameterized by 4 leg lengths $\ell^{(a)}$ and an opening angle θ (Fig. 1*B*). A pantograph lattice then, is a two-dimensional array of scissors $\{\boldsymbol{S}_{i,j}\}$ with two types of joints: 1) scissor pivots $\boldsymbol{p}_{i,j}$ (orange) join the legs of a single scissor, while 2) vertex pivots $\boldsymbol{x}_{i,j}$ (blue) connect pairs of legs at their tips (Fig. 1*G*). We treat scissor pivots as revolute joints and vertex pivots as spherical joints (i.e., they constrain the position of connected rods but not their orientation — see Fig. 1 *H* and *I*).

We will also find it useful to refer to the leg vectors ($\boldsymbol{v}_{i,j}^{(1)} \stackrel{\text{def}}{=} \left(\boldsymbol{p}_{i,j} - \boldsymbol{x}_{i,j}\right)/\|\boldsymbol{p}_{i,j} - \boldsymbol{x}_{i,j}\|$, $\boldsymbol{v}_{i,j}^{(2)} \stackrel{\text{def}}{=} \left(\boldsymbol{p}_{i,j} - \boldsymbol{x}_{i,j+1}\right)/\|\boldsymbol{p}_{i,j} - \boldsymbol{x}_{i,j+1}\|$) which point along the direction of each leg, and edge vectors ($\boldsymbol{e}_{i,j} \stackrel{\text{def}}{=} \boldsymbol{x}_{i+1,j} - \boldsymbol{x}_{i,j}$ and $\boldsymbol{h}_{i,j} \stackrel{\text{def}}{=} \boldsymbol{x}_{i,j+1} - \boldsymbol{x}_{i,j}$) which lie along the boundary of each scissor (note that both the edge and leg vectors are a function of θ).

We finally define the kinematic configuration of a pantograph lattice as the set of opening angles: $\mathbf{C} \stackrel{\text{def}}{=} \left\{\theta_{i,j}\right\}$. Immediately we observe that the opening angles of adjacent scissors are coupled: opening/closing $\boldsymbol{S}_{ij}$ controls its immediate neighbors $\left\{\boldsymbol{S}_{i\pm1,j\pm1}\right\}$, which in turn percolates to all scissors in the lattice. The kinematic configuration can thus be smoothly parameterized by a scalar Θ such that $\mathbf{C}(\Theta) = \left\{\theta_{i,j}(\Theta)\right\}$.

As previously stated, the main result of this paper is a method to design pantograph lattices which are 1) deployable, 2) collapsible, and 3) rigid-embeddable. We now discuss each of these constraints in detail.

Deployability. An arbitrary set of scissors cannot be joined into a pantograph lattice, let alone reconfigured between multiple states. To tease out the conditions for deployability we will first

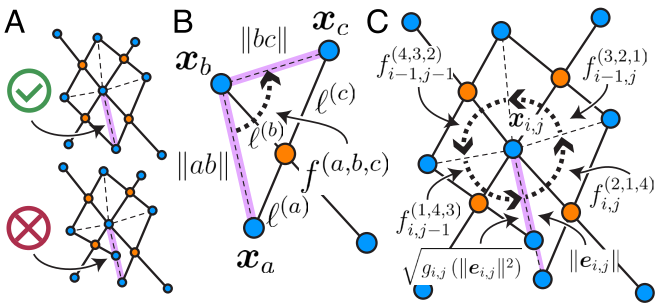

Fig. 2. Intrinsic compatibility. (*A*) A set of four scissors satisfy intrinsic compatibility if the lengths of all adjacent edges are equal (see highlighted edge). (*B*) The squared edge lengths $\|ab\|^2$ and $\|bc\|^2$ are related by an affine function which only depends on leg lengths (Eq. **1**). (*C*) We can derive a closure condition for intrinsic compatibility by considering mapping facet edge lengths around an enclosed vertex $\boldsymbol{x}_{i,j}$ (Eq. **3**).

consider the simplest nontrivial pantograph lattice consisting of four scissors joined with a single vertex pivot into a 2×2 assembly as shown in Fig. 2*A*.

We will say that a set of scissors satisfies intrinsic compatibility if, for some configuration $\boldsymbol{C}(\Theta)$, edges of all abutting scissors are equal.* Intrinsic compatibility is a closure condition associated with the coupling of opening angles between scissors which form a loop around a central vertex pivot (Fig. 2*A*).

Referring to Fig. 2*B*, consider three legs of a scissor with endpoints at $\boldsymbol{x}_a$, $\boldsymbol{x}_b$, $\boldsymbol{x}_c$ and let $\|ab\|$ and $\|bc\|$ be the length of two adjacent edges (i.e., they share $\boldsymbol{x}_b$ in common). There is an affine relationship (Eq. **1**) between the squared lengths of these edges in terms of the scissor leg lengths (see *SI Appendix*, section S.I.A for full derivation)

$$\|bc\|^2 = f^{(a,b,c)}(\|ab\|^2) \stackrel{\text{def}}{=} \gamma^{(a,b,c)} - \eta^{(b,c)}\|ab\|^2. \quad [1]$$

In Eq. **1** we have assumed $0 < \theta < \pi/2$ and introduced the symbols $\gamma^{(a,b,c)} \stackrel{\text{def}}{=} \ell^{(b)^2} + \ell^{(c)^2} + \eta^{(a,c)}\left(\ell^{(a)^2} + \ell^{(b)^2}\right)$ and $\eta^{(a,c)} \stackrel{\text{def}}{=} \frac{\ell^{(c)}}{\ell^{(a)}}$). Returning to a full lattice of scissors, Eq. **1** allows us to write down a relationship between the lengths of any two edges which share a vertex, for example $\boldsymbol{e}_{i,j}$ and $\boldsymbol{h}_{i,j}$ are related by $\|\boldsymbol{h}_{i,j}\|^2 = f^{(2,1,4)}_{i,j}(\|\boldsymbol{e}_{i,j}\|^2)$ (subscripts of f indicate the scissor under consideration).

We now turn to a set of four scissors arranged around vertex $\boldsymbol{x}_{i,j}$, as illustrated in Fig. 2*C*. By recursively applying Eq. **1** we can propagate $\|\boldsymbol{e}_{i,j}\|^2$ in a full loop around vertex $\boldsymbol{x}_{i,j}$, a "loop" operation we name $g_{i,j}$ (Fig. 2*C*).

$$g_{i,j}(\|\boldsymbol{e}_{i,j}\|^2) \stackrel{\text{def}}{=} f^{(1,4,3)}_{i,j-1} \circ f^{(4,3,2)}_{i-1,j-1} \circ f^{(3,2,1)}_{i-1,j} \circ f^{(2,1,4)}_{i,j}\left(\|\boldsymbol{e}_{i,j}\|^2\right). \quad [2]$$

Now recall that the lengths of the edge vectors in a pantograph lattice are a function of the configuration $\mathbf{C}(\Theta)$ (since different configurations correspond to different states of opening/closing the scissors). Thus, a 2×2 scissor lattice satisfies intrinsic compatibility in a state $\mathbf{C}(\Theta)$ if and only if $g_{i,j}$ is the identity operation (Eq. **3**).

$$g_{i,j}(\|\boldsymbol{e}_{i,j}\|^2) = \|\boldsymbol{e}_{i,j}\|^2. \quad [3]$$

We can extend the notion of intrinsic compatibility to an $M \times N$ scissor lattice by requiring that Eq. **3** is satisfied for all $\{i,j | 0 < i \le M, 0 < j \le N\}$ (that is, we require every 2×2 sublattice independently satisfies intrinsic compatibility).

A 2×2 or larger scissor lattice is geometrically overconstrained, and additional symmetries are required to introduce kinematic degrees of freedom (21). We will say that a lattice is deployable between two states Θ_0 and Θ_1 if it satisfies intrinsic compatibility over the continuous range of states between them: $\{\boldsymbol{C}(\Theta) | \Theta_0 < \Theta < \Theta_1\}$. The following lemma simplifies the search for lattices that satisfy this condition:

Lemma 1. *If a 2×2 scissor mechanism satisfies intrinsic compatibility in two distinct states $\boldsymbol{C}(\Theta_0)$, $\boldsymbol{C}(\Theta_1)$ with $\Theta_0 < \Theta_1$ the mechanism satisfies intrinsic compatibility in all intermediate states $\{\boldsymbol{C}(\Theta) | \Theta_0 < \Theta < \Theta_1\}$.*

Proof: Observe that g is an affine function since it is a composition of affine functions. Given that g is affine and since Eq. **3** is satisfied for two different states ($\boldsymbol{C}(\Theta_0)$ and $\boldsymbol{C}(\Theta_1)$, by assumption), it must be the case that g is the identity map (i.e., $g(\|\boldsymbol{e}\|^2) = \|\boldsymbol{e}\|^2$ for all values of $\|\boldsymbol{e}\|$). Thus intrinsic compatibility holds for all states $\{\boldsymbol{C}(\Theta) | \Theta_0 < \Theta < \Theta_1\}$ and the mechanism is deployable over this range. □

We now extend this argument to generic pantograph structures (e.g., Fig. 1*G*).

Theorem 1. *If a $M \times N$ ($M \ge 2$ and $N \ge 2$) scissor mechanism satisfies intrinsic compatibility in two distinct states $\boldsymbol{C}(\Theta_0)$, $\boldsymbol{C}(\Theta_1)$ with $\Theta_0 < \Theta_1$, the mechanism is deployable between Θ_0 and Θ_1.*

Proof: Consider any 2×2 sublattice: $\{\boldsymbol{S}_{i,j}, \boldsymbol{S}_{i,j+1}, \boldsymbol{S}_{i+1,j}, \boldsymbol{S}_{i+1,j+1}\}$ where $i \in (0, M-1), j \in (0, N-1)$. Since there are two distinct deployed states ($\mathbf{C}(\Theta_0)$, $\mathbf{C}(\Theta_1)$) for the entire lattice, this immediately implies there are two distinct deployed states for the 2×2 sublattice. Lem. 1 implies that this sublattice satisfies intrinsic compatibility for all intermediate states. Since this holds for all possible sublattices, the entire $M \times N$ lattice also satisfies intrinsic compatibility for all states $\{\boldsymbol{C}(\Theta) | \Theta_0 < \Theta < \Theta_1\}$ and thus is deployable over this range. □

In practical terms, if a pantograph lattice has two distinct states which are intrinsically compatible, Theorem 1 proves that it can be deployed between them. Theorem 1 however does not imply the lattice can be deployed to states outside of $[\Theta_0, \Theta_1]$ as scissors may pass through a terminal state (either $\theta = 0$ or $\theta = \pi$) (For further discussion see *SI Appendix*, section S.I.B). In passing, we note that this two-state condition for deployability is analogous to the condition for foldability of four-coordinated origami vertices (22).

Collapsibility. We now introduce a geometric constraint which we term collapsibility that describes whether a scissor-based structure can be completely "flattened" with all bars parallel to one another as illustrated in Fig. 3*A*. To derive the collapsibility conditions for a lattice of scissors, consider the gaps formed between the legs of scissors which are joined by a pair of vertex pivots (either vertically or horizontally) as illustrated in Fig. 3*B*. In order for all scissors to fold to a state $\theta_{i,j} = 0$ the sum of the

*Of course, it is straightforward to design lattices of scissors which satisfy intrinsic compatibility: start with a quadrilateral mesh and draw diagonals to construct the pivot center and legs. However, structures designed in this manner will be generically rigid as we discuss later in this section.

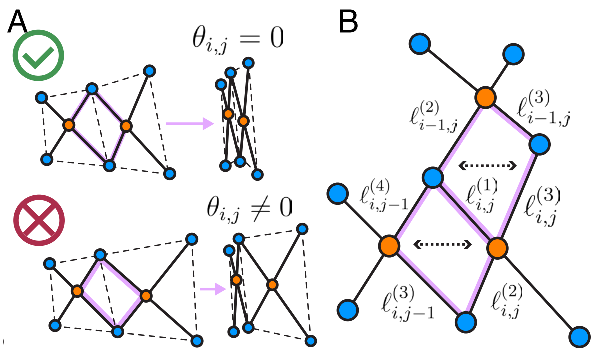

Fig. 3. Collapsibility. (*A*) Collapsibility describes whether a pantograph structure can be completely "flattened" with all opening angles $\theta_{i,j} = 0$. Note that in the lower example the left scissor achieves $\theta = 0$ while the right scissor is limited to a state $\theta > 0$. Therefore, the system is not collapsible. (*B*) Collapsibility requires that the combined length of the legs on the left and right of each pore formed between two scissors must be equal (Eq. **4**).

length of legs on the left of each pore must equal the sum of the lengths of the legs on the right.[†]

$$\ell^{(3)}_{i,j-1} + \ell^{(4)}_{i,j-1} = \ell^{(1)}_{i,j} + \ell^{(2)}_{i,j} \qquad (\boldsymbol{S}_{i,j-1} \text{ and } \boldsymbol{S}_{i,j}) \qquad \textbf{[4a]}$$

$$\ell^{(2)}_{i-1,j} + \ell^{(1)}_{i,j} = \ell^{(3)}_{i-1,j} + \ell^{(4)}_{i,j} \qquad (\boldsymbol{S}_{i-1,j} \text{ and } \boldsymbol{S}_{i,j}). \qquad \textbf{[4b]}$$

Analogous to the role of developability in origami (6) or contractibility in kirigami (7), collapsibility here specifies the geometry of a terminal kinematic state. Eq. **4** generalizes the collapsibility conditions for a one-dimensional chain of scissors found by ref. 23.

Rigid-Embeddability. In order to treat the deployed morphology of pantograph lattices from a purely geometric perspective, without recourse to the energetics of bending or twisting, we finally require that scissors are rigidly embedded in the deployed configuration (that is, scissor legs are straight).[‡] Unfortunately, this is difficult to ensure from purely intrinsic quantities as it requires global, origami-like coordination of the dihedral angles between scissors (folding about $\boldsymbol{e}$ and $\boldsymbol{h}$ vectors). As we will show in the following section, we circumvent this challenge by designing lattices directly in a rigid-embedded deployed configuration.

Additive Construction

The preceding definitions formalize the design space of pantograph lattices. One could, in theory, now search for lattices with a given shape which are deployable and collapsible through various constrained optimization approaches. In the next section of this paper we present a protocol which greatly simplifies this process by analytically parameterizing the space of all possible pantograph structures.

The key insight is to formulate design as an additive construction problem. That is, given an existing pantograph lattice, we ask how to attach a new set of scissors along a boundary such that the resulting structure preserves these properties. Our solution, illustrated schematically in Fig. 4*A* and formalized by Theorem 2 adds one scissor at a time along a boundary until an entire new row is constructed.

This method satisfies all three constraints previously introduced. First, as we design the pantograph lattice directly in the deployed configuration, we guarantee rigid embeddability. Simultaneously, our method satisfies Eq. **4** and ensures the coexistence of a collapsed state as an integral part of our construction. Finally, since we know the structure satisfies intrinsic compatibility in two states (collapsed and deployed) Theorem 1 guarantees that the lattice is deployable between them.

We begin by defining a growth front F as an ordered set of connected scissor edges of the same type (that is, either $\boldsymbol{e}$- or $\boldsymbol{h}$-like) along a boundary of a pantograph lattice. For example, in Fig. 4 *A.1* we highlight an $\boldsymbol{h}$-like growth front at the lower boundary of the pantograph lattice $F = \{\boldsymbol{h}_{i,j} | 0 < j \leq N\}$.

Theorem 2. *The space of scissors pivots along a growth front F of a pantograph lattice in D dimensions has* $(D-1)$ *DOF and is parameterized by the choice of one leg direction at any edge along a front.*

Proof: We will discuss construction along a $\boldsymbol{h}$-like growth front $F = \{\boldsymbol{h}_{i,j} | 0 < j \leq N\}$ (Fig. 4 *A.1*) while an analogous proof for $\boldsymbol{e}$-like fronts is presented in *SI Appendix*, section S.II.B. Our proof can be broken down into three steps: first, conditions for construction of a single scissor pivot $\boldsymbol{p}_{i,j}$ attached to $\boldsymbol{h}_{i,j}$ (Fig. 4 *A.2*); second, construction of adjacent scissor pivots $\boldsymbol{p}_{i,j\pm1}$ (Fig. 4 *A.3*); and finally construction of all scissor pivots along a growth front (Fig. 4 *A.4*). ☐

Construction of a single scissor pivot. Consider adding a scissor pivot to edge $\boldsymbol{h}_{i,j}$ as illustrated in Fig. 4 *B.1*. To begin the construction, we first specify the leg direction $\boldsymbol{v}^{(2)}_{i,j}$ (Fig. 4 *B.2*). Now, the lengths $\ell^{(1)}_{i,j}$, $\ell^{(4)}_{i,j}$ and the remaining leg direction $\boldsymbol{v}^{(1)}_{i,j}$ are coupled by the vector closure condition highlighted in Fig. 4 *B.3* and given by Eq. **5** so all three are determined once any one is known.

$$\ell^{(1)}_{i,j}\boldsymbol{v}^{(1)}_{i,j} = \boldsymbol{h}_{i,j} + \ell^{(4)}_{i,j}\boldsymbol{v}^{(2)}_{i,j}. \qquad \textbf{[5]}$$

$\ell^{(1)}_{i,j}$ and $\ell^{(4)}_{i,j}$ must also satisfy the relevant collapsibility relations between $\boldsymbol{S}_{i-1,j}$ and $\boldsymbol{S}_{i,j}$ (Eq. **4**b). Solving Eqs. **5** and **4**b for $\ell^{(4)}_{i,j}$ we find:

$$\ell^{(4)}_{i,j} = \frac{{\kappa^{(h)}_{i,j}}^2 - ||\boldsymbol{h}_{i,j}||^2}{2\left(\kappa^{(h)}_{i,j} + \boldsymbol{h}_{i,j} \cdot \boldsymbol{v}^{(2)}_{i,j}\right)}. \qquad \textbf{[6]}$$

Here we introduce a constant $\kappa^{(h)}_{i,j} \stackrel{\text{def}}{=} \ell^{(2)}_{i-1,j} - \ell^{(3)}_{i-1,j}$, which quantifies the asymmetry between the legs of scissors attached to $\boldsymbol{h}_{i,j}$—that is, both the existing scissor $\boldsymbol{S}_{i-1,j}$ and the scissor under construction $\boldsymbol{S}_{i,j}$. Now, given $\ell^{(4)}_{i,j}$ we can construct $\boldsymbol{p}_{i,j} = \boldsymbol{x}_{i,j+1} + \ell^{(4)}_{i,j}\boldsymbol{v}^{(2)}_{i,j}$ (Fig. 4 *B.4*). For derivation of Eq. **6** and geometric interpretation see *SI Appendix*, section S.II.A.

If $N = 1$ there are no further pivots to construct and the only freedom we have is to set the direction of a single leg vector

[†] We note that an alternate collapsed state may exist in which the scissors are fully "opened" in the sense that for some Θ_o, we have $\mathbf{C}(\Theta_o) = \pi$ (*SI Appendix*, Eq. **S.1** gives the formulas analogous to Eq. **4** for π-collapsibility). As the conditions for 0- and π- collapsibility are equivalent up to a change of coordinates $\theta \to \pi - \theta$ we will simply refer to collapsibility in the sense defined above.

[‡] Indeed, rigid-embeddability was already implicit in our notation in Fig. 1*G* as we used only two leg vectors—$\boldsymbol{v}^{(1)}$ and $\boldsymbol{v}^{(2)}$—to describe the orientation of all four legs.

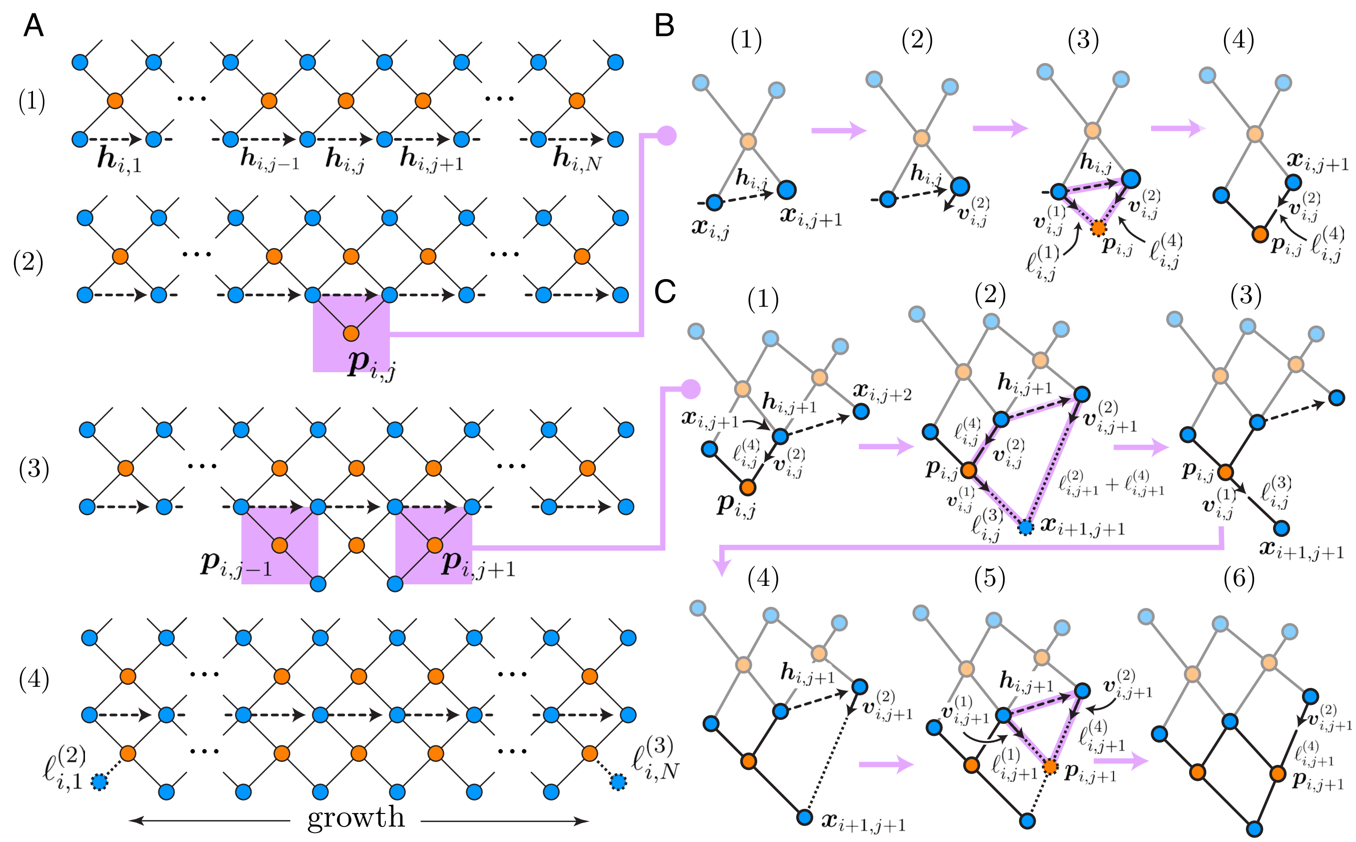

Fig. 4. Construction of a row of scissors. (*A*) Overview of the method. (*A.1*) An $\boldsymbol{h}$-like growth $\{\boldsymbol{h}_{i,1},\ldots,\boldsymbol{h}_{i,N}\}$. (*A.2*) Construction of a single pivot ($\boldsymbol{p}_{i,j}$) attached to $\boldsymbol{h}_{i,j}$. See (*B*) for detail. (*A.3*) Construction of neighboring pivots ($\boldsymbol{p}_{i,j+1}$ and $\boldsymbol{p}_{i,j-1}$). See (*C*) for detail. (*A.4*) Continue construction for all sites along the front. $\ell^{(2)}_{i,1}$, $\ell^{(3)}_{i,N}$ are free parameters not fixed by the scissor pivot construction. (*B*) Detailed construction of a single scissor pivot. (*B.1*) Initial set up. (*B.2*) One leg direction (here, $\boldsymbol{v}^{(2)}_{i,j}$) can be chosen freely. (*B.3*) The location of the new pivot must satisfy both the highlighted vector closure condition (Eq. **5**) and collapsibility. Solving for these conditions we calculate $\ell^{(4)}_{i,j}$ (Eq. **6**). (*B.4*) Completed construction. (*C*) Construction of scissor pivot at adjacent edge $\boldsymbol{h}_{i,j+1}$. (*C.1*) Initial set up. (*C.2*) The location of vertex $\boldsymbol{x}_{i+1,j+1}$ must satisfy both a vector closure condition (highlighted) and collapsibility. Solving these conditions we isolate $\ell^{(3)}_{i,j}$ (*SI Appendix*, section S.II.A). (*C.3*) $\ell^{(3)}_{i,j}$ fixes position of $\boldsymbol{x}_{i+1,j+1}$. (*C.4*) $\boldsymbol{x}_{i+1,j+1}$ fixes the direction of $\boldsymbol{v}^{(2)}_{i,j+1}$. (*C.5*) We apply the same construction used for $\boldsymbol{p}_{i,j}$ to find $\boldsymbol{p}_{i,j+1}$ given leg direction $\boldsymbol{v}^{(2)}_{i,j+1}$ (see *B*, above) (*C.6*) Completed construction of $\boldsymbol{p}_{i,j+1}$.

($\boldsymbol{v}^{(2)}_{i,1}$) which has $(D-1)$ DOF.[§] In the case $N>1$, we will show that the locations of the adjacent scissor pivots ($\boldsymbol{p}_{i,j-1}, \boldsymbol{p}_{i,j+1}$) are coupled by the collapsibility equations (Eq. **4**) associated with the corresponding scissors ($\boldsymbol{S}_{i,j}, \boldsymbol{S}_{i,j+1}$).

Construction of adjacent pivots. The location of $\boldsymbol{p}_{i,j}$ uniquely determines that of its neighbors, $\boldsymbol{p}_{i,j\pm1}$. Here we show the construction for $\boldsymbol{p}_{i,j+1}$ (Fig. 4*C*), while the symmetric argument for $\boldsymbol{p}_{i,j-1}$ is given in *SI Appendix*, section S.II.A.

First, we construct vertex pivot $\boldsymbol{x}_{i+1,j+1}$ (Fig. 4 *C.1–C.3*). Analogous to the construction of $\boldsymbol{p}_{i,j}$ given above, we combine a vector closure relation (highlighted in Fig. 4 *C.2*) with the relevant set of collapsibility conditions (associated with $\mathbf{S}_{i,j}$, $\mathbf{S}_{i,j+1}$, and $\mathbf{S}_{i-1,j+1}$) and solve for $\ell^{(3)}_{i,j}$ (details in *SI Appendix*, section S.II.A). The location of $\boldsymbol{x}_{i+1,j+1}$ is then given by $\boldsymbol{x}_{i+1,j+1}=\boldsymbol{p}_{i,j}+\ell^{(3)}_{i,j}\boldsymbol{v}^{(1)}_{i,j}$ (Fig. 4 *C.3*).

The position of $\boldsymbol{x}_{i+1,j+1}$ fixes $\boldsymbol{v}^{(2)}_{i,j+1}$ (Fig. 4 *C.4*). Thus, we can apply the previously derived construction for $\boldsymbol{p}_{i,j}$ to establish the location of $\boldsymbol{p}_{i,j+1}$ (compare Fig. 4 *B.3* and *B.4* and Fig. 4 *C.5* and *C.6*).

Growth along entire front. Iterating the preceding construction along F allows us to assemble the full row of scissor pivots one at a time. More formally, we see that the geometric construction of $\boldsymbol{p}_{i,j\pm1}$ from $\boldsymbol{p}_{i,j}$ corresponds to a bijective and invertible transfer function $\tau_{i,j}$ which maps adjacent scissor pivot locations:

$$\boldsymbol{p}_{i,j+1}=\tau_{i,j}\left(\boldsymbol{p}_{i,j}\right). \quad [7]$$

Now consider constructing $\boldsymbol{p}_{i,j'}$ given $\boldsymbol{p}_{i,j}$ assuming $j'>j$. We can do so using a composition of transfer functions:

$$\boldsymbol{p}_{i,j'}=\tau_{i,j'-1}\circ\tau_{i,j'-2}\circ\cdots\tau_{i,j+1}\circ\tau_{i,j}(\boldsymbol{p}_{i,j}). \quad [8]$$

As all τ are bijective, their composition is bijective and thus all scissor pivots on the front $\left\{\boldsymbol{p}_{i,j'}|0<j'\leq N\right\}$ are fixed by the location of any pivot on the front $\boldsymbol{p}_{i,j}$, which is in turn set by the choice of a single leg direction $\boldsymbol{v}^{(2)}_{i,j}$. Thus, for a front F with N scissors ($N\geq1$), the space of possible new scissor pivot locations is set by one leg direction, which has $(D-1)$ degrees of freedom.

§We could have equivalently proceeded by setting $\boldsymbol{v}^{(1)}_{i,j}$. See *SI Appendix*, section S.II.A for corresponding derivation.

Note that the method demonstrated above fixes not only the position of a new set of scissor pivots but also the vertex pivots $\{\boldsymbol{x}_{i+1,j} | 1 < j \leq N\}$ and leaves only $\boldsymbol{x}_{i+1,1}$ and $\boldsymbol{x}_{i+1,N+1}$ indeterminate (up to a choice of $\ell_{i,1}^{(2)}$ and $\ell_{i,N}^{(3)}$). Thus, to fully specify the row of scissors attached to F, we have the freedom to choose one leg direction (e.g., $\boldsymbol{v}_{i,j}^{(2)}$) and the length of the two legs on the boundary (Fig. 4 *A.4*).

Extrinsic Algorithm. Given an existing pantograph lattice, Theorem 2 guarantees we can augment it with a new row of scissors such that the resulting lattice continues to satisfy deployability, collapsibility, and rigid-embeddability. This suggests a natural procedure to design pantograph lattices by iterative construction—a procedure we name the Extrinsic Algorithm.

As a concrete example, consider constructing a 3×5 pantograph lattice as illustrated in Fig. 5*A*. We begin by specifying a minimal seed (Fig. 5 *A.1*) which consists of 1) an initial growth front $\{\boldsymbol{h}_{1,j} | 0 < j \leq 4\}$ and 2) a corresponding set of $\{\kappa_{1,j}^{(h)} | 0 < j \leq 4\}$. Given the seed we can construct the first row of scissors $\{\boldsymbol{S}_{1,1}, \ldots, \boldsymbol{S}_{1,4}\}$ by applying the method developed in our proof of Theorem 2 to construct a row of pivots $\{\boldsymbol{p}_{1,j} | 0 < j \leq 4\}$ (Fig. 5 *A.2*). To complete this row, we must also specify the initial and final leg lengths ($\ell_{1,1}^{(2)}$ and $\ell_{1,4}^{(3)}$). At each subsequent steps of construction, we select a new growth front and repeat this process (Fig. 5 *A.3–A.5*). Note that we are able to grow from any boundary of the lattice, including both $\boldsymbol{h}$- (steps 1, 2, and 4) and $\boldsymbol{e}$- (step 3) fronts.

The extrinsic algorithm can be summarized as follows:

1. Specify initial seed ($\{\boldsymbol{h}_{1,j}\}$ and $\{\kappa_{1,j}^{(h)}\}$).¶
2. Pick a growth front F.
3. Design row of scissors pivots attached to F.
   (a) Pick a single leg direction at any edge along the front.
   (b) Propagate along front.
4. Specify free leg lengths.
5. Repeat 2–4 until complete.

As initial conditions are arbitrary (step 1) and the construction of each additional row satisfies Theorem 2 (steps 2–5), the extrinsic algorithm explores the space of all possible pantograph lattice structures (which satisfy deployability, collapsibility, and rigid-embeddability). This further shows that the space of pantograph lattices designable from a given initial seed is independent of the sequence of growth fronts chosen during construction. For instance, in the example illustrated in Fig. 5*A* the direction of growth picked for steps (1–4) could be reordered and still result in the final form shown in (5).

We can also apply the extrinsic construction to alternative lattice topologies in which we identify opposite edges to form a cylinder, or adjacent rows to form a helix (discussion in *SI Appendix*, section S.III). Additional constraints (e.g., requirements for fabrication) can also be wrapped into this construction algorithm by imposing limits on the choice of leg direction or free leg lengths.

We now present a set of examples which demonstrate the flexibility of the extrinsic algorithm (26). For all designs, we also show desktop-scale physical realizations (see *Materials and Methods* for details).

First, we approximate a flat disk (Fig. 5*B*). Here we take the position of the initial seed (given in term of vertex pivots) $\{\boldsymbol{x}_{1,j}\}$, one leg direction per row $\{\boldsymbol{v}_{i,1}^{(2)}\}$, and the boundary leg lengths of each row as variables and search for configurations in which boundary vertices lie on the circumference of the target disk. We use a similar procedure to approximate the three-dimensional surface of a half ellipsoid (Fig. 5*C*). (See *SI Appendix*, section S.V for details of the fitting procedure.) We note that other optimization schemes or fitting metrics may lead to other valid approximations for the same surface and our purpose here is merely to demonstrate that our additive procedure is amenable to inverse design problems. Crucially, our algorithm transforms the naive design problem, which consists of an optimization over $\mathcal{O}(M \times N)$ parameters (i.e., leg lengths) with $\mathcal{O}(M \times N)$ equality constraints (due to collapsibility) to an optimization over $\mathcal{O}(M + N)$ free parameters—the choice of one leg direction per row plus the boundary leg lengths. Further, since the extrinsic algorithm is purely geometric in origin this optimization process requires no computationally expensive physical simulation.

For our next two examples, we explore two alternative pantograph lattice topologies (details in *SI Appendix*, section S.V). First, we design a cylindrical pantograph lattice which approximates a torus (Fig. 5*D*). Here the initial seed consists of 12 equally spaced points along the nodal line of the torus, while subsequent rows are chosen to map successive loops around the waist.# Finally, we construct a helical pantograph lattice with loop length $N = 12$ which is grown for 18 steps at both ends (Fig. 5*D*).

Intrinsic Algorithm. Our additive procedure can be extended to directly program the intrinsic geometry of a pantograph lattice without reference to an extrinsic embedding (Fig. 6).

To motivate this step, recall that our goal in designing the additive algorithm was to preserve deployability, collapsibility, and rigid embeddability. If we now relax the rigid-embeddability constraint (while preserving both deployability and collapsibility) we find that we can apply an arbitrary rotation to every edge along the growth front before constructing the next row of scissors. More formally, consider a growth front of length N: $F = \{\boldsymbol{h}_{i,j} | 0 < j \leq N\}$ and a set of N rotation matrices $\{R_j | 0 < j \leq N\}$. A compatible growth front $\tilde{F}$ can be designed by applying rotation R_j to edge $\boldsymbol{h}_{i,j}$ such that $\tilde{F} \overset{\text{def}}{=} \{R_j \boldsymbol{h}_{i,j}\}$. For geometric intuition, the space of compatible fronts $\{\tilde{F}\}$ corresponds to all possible orientations of a discrete curve with the same edge lengths as the original front F.

We can now perform additive construction with compatible growth fronts, a procedure we name the Intrinsic Algorithm. The intrinsic algorithm follows the same steps as the extrinsic algorithm, replacing the front F with a compatible growth front $\tilde{F}$ (see *SI Appendix*, section S.IV for details). As a minimal demonstration, we design three 2×2 pantograph lattices which exhibit positive, zero, and negative Gaussian curvature (Fig. 6*B*). All examples start with an identical pair of scissors (and hence identical growth front F). We then design a different compatible growth front ($\tilde{F}$) to achieve the desired curvature defects (detail in *SI Appendix*, section S.IV).

We demonstrate two larger structures designed using the intrinsic algorithm (26). In Fig. 6*C*, we show a surface of mixed curvature inspired by the origami eggbox pattern. Here regions of

¶This choice of seed implies the initial growth front is $\boldsymbol{h}$-like. Initialization with an $\boldsymbol{e}$-like front is analogous, see §S.II.

#More generally, any axisymmetric surface (free of self-crossings) admits a pantograph lattice approximation. See *SI Appendix*, section S.III).

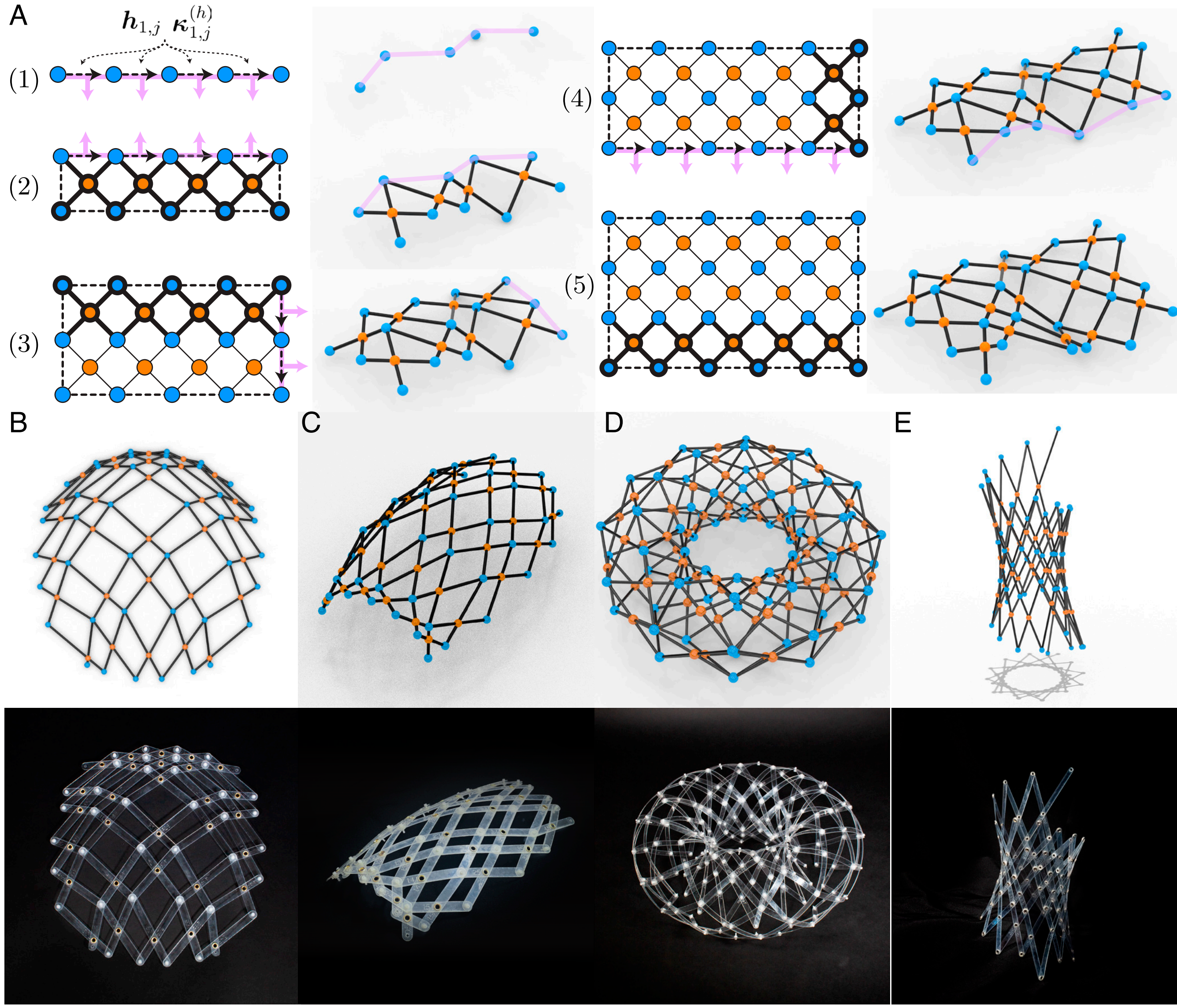

Fig. 5. Additive algorithm. (*A*) Step-by-step construction of a 3×5 pantograph lattice. At each stage we illustrate the topology (left column) and deployed geometry (right column). In the topological diagrams dotted lines around the boundary indicate possible growth fronts, the highlighted line indicates front used in next step of construction, and bold scissors indicate the row/column added by the preceding step of construction. (*A.1*) The initial seed for construction consists of a set of vertices $\{\boldsymbol{x}_{0,j}\}$ and collapsibility $\{\kappa_{0,j}^{(h)}\}$ values. (*A.2–A.5*) Each subsequent step of construction adds a row or column of scissors along a boundary. (*B* and *E*) A sample of pantograph lattices designed using the additive algorithm and physical realizations. (*B* and *C*) Pantograph lattices which map the surface a disk and a half ellipsoid, respectively. To design these models we start with a seed on the boundary and optimize over the free parameters of each row (initial pivot locations and terminal leg lengths) to fit the target shapes. (*D*) A cylindrical pantograph lattice that approximates an axisymmetric torus. (*E*) A helical pantograph lattice grown from a helical seed ($N = 12$) with 18 steps of growth at both ends.

positive curvature are multistable, and can be "popped through," while collapsing the lattice removes the curvature defects and resets the system to an initial state. In Fig. 6*D*, we design a surface of constant negative discrete Gaussian curvature, using a sequence of identical subunits which can be repeated in a loop to form one ring of the final structure (see *SI Appendix*, section S.V for additional detail on designs). This surface is analogous to those demonstrated by Ono et al. (24, 25) but exemplifies the formalism for programming intrinsic curvature developed in this work.

Deployment and Mechanics

We conclude our paper by discussing the behavior of pantograph lattices during deployment. We find all of our physical models transform smoothly between collapsed and deployed states (Movies S1–S6); to gain further intuition we performed spring-and-ball simulations (*Materials and Methods*) to characterize the energetics of this process, which we report in *SI Appendix*, section S.VI. While a full study of deployment mechanics and energetics would require material specific elastic calculations beyond the scope of this paper, our results suggest that pantograph lattices designed with the extrinsic algorithm may pass through states of geometric frustration analogous to those present when folding or unfolding origami structures (4, 5). This is perhaps unsurprising, as the additive procedure only guarantees global rigid-embeddability in the initial and final configurations and deployment through a non-rigid-embeddable configuration would introduce bending or twisting of scissor legs. Similarly, we find evidence that lattices designed with the intrinsic algorithm

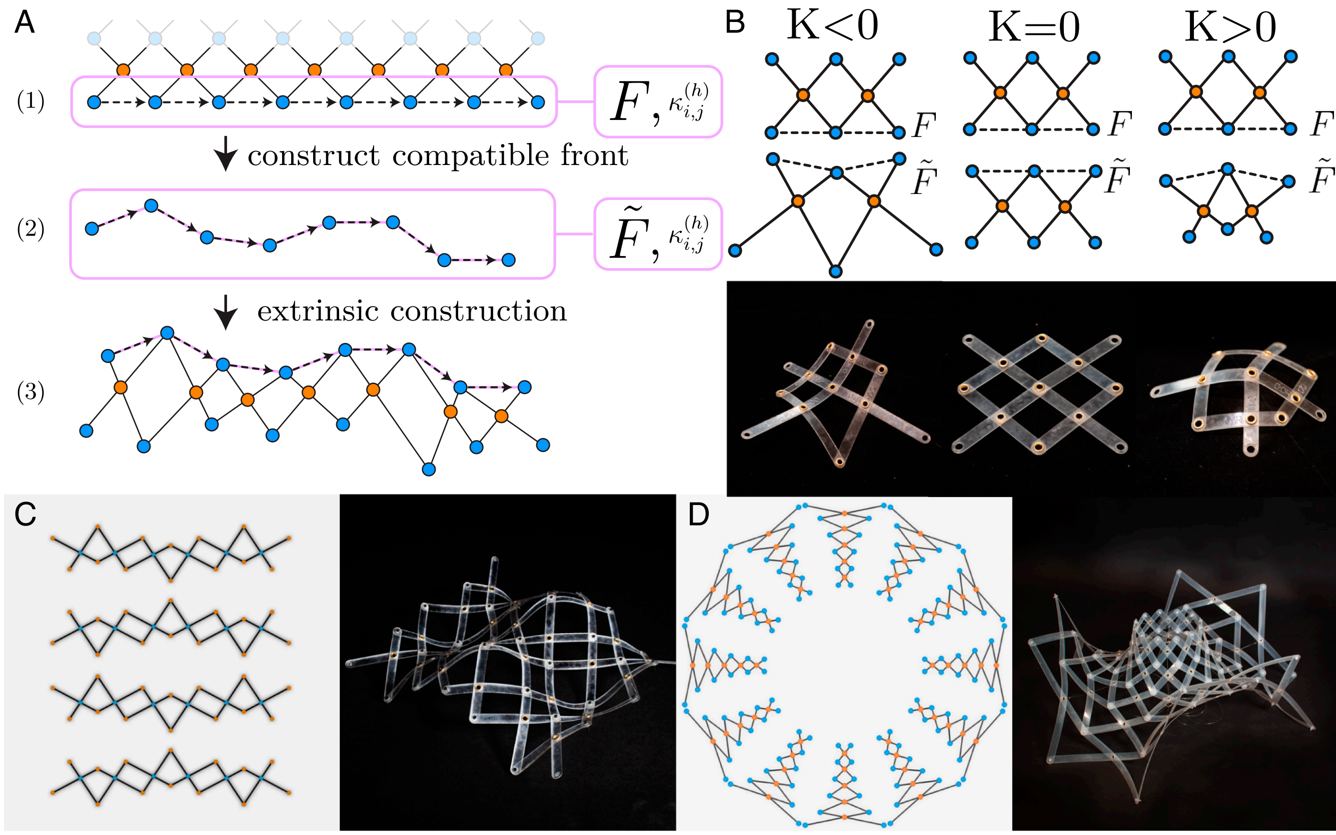

Fig. 6. Intrinsic algorithm. (*A*) We can generalize the additive procedure by considering a class of compatible growth fronts. (*A.1*) A growth front $F = \{\boldsymbol{h}_{i,j}\}$ and associated $\{\kappa_{i,j}^{(h)}\}$. (*A.2*) A compatible growth front is given by any space curve with the same sequence of edge lengths. (*A.3*) Given a compatible front F we can apply the extrinsic algorithm to construct a strip of scissors compatible with the original pantograph structure. (*B*) Construction of positive, zero, and negative curvature defects in a 2×2 pantograph lattice. (*C* and *D*) Demonstrations of pantograph lattices designed using the intrinsic algorithm. (*C*) An eggbox-like surface with multistable "nodes" which can be flipped in the deployed state (and reset by closing the structure). (*D*) A surface of constant negative discrete Gaussian curvature.

may have nonzero energy in the deployed configuration, which corresponds to the fact that the intrinsic algorithm does not guarantee rigid-embeddability and hence geometric frustration may persist in the deployed configuration.

Conclusions

Inspired by the simple shearing motion of a pair of scissors, we have provided a method to characterize, design, and build a class of linkage-based geometric metamaterials we name pantograph lattices. The geometric constraints underpinning these structures allowed us to characterize the full space of collapsible and deployable scissor lattices and to construct a rich menagerie of surfaces in two and three dimensions. By introducing an additive design framework—first in extrinsic form and then as an intrinsic generalization—we reduced the global design problem to a sequence of local, analytically solvable steps. In doing so, we showed that the space of pantograph lattices is both orderly and generative: simple rules applied iteratively can realize planar, curved, cylindrical, and helical surfaces; encode curvature defects; and produce multistable nodes and features (e.g., the eggbox-like designs in Fig. 6). At a practical level, this construction enables straightforward computational exploration and, through our multimaterial 3D-printing scheme, automated fabrication of fully assembled morphable mechanisms (Fig. 7).

Looking ahead, this geometric framework opens several directions. One natural next step lies in marrying geometry with mechanics. As our bead-and-spring simulations suggest, pantograph lattices may exhibit controlled geometric frustration during deployment, raising the possibility of programming energy landscapes, snap-through transitions, multistability, or shape-dependent stiffness into their design. Another direction is scaling: because the construction is purely geometric and relies only on local constraints, pantograph lattices invite translation from microdevices to architectural systems, echoing the breadth found in origami- and kirigami-based metamaterials. More broadly, the interplay between additive geometric growth, intrinsic compatibility, and curvature programming hints at deeper connections to discrete differential geometry and deployable structures. We anticipate that pantograph lattices will become part of a growing vocabulary of programmable matter, providing a bridge between classical linkage mechanisms and modern geometric metamaterials.

Materials and Methods

Physical Fabrication. We explore two methods to fabricate desktop scale pantograph lattices.

The first, used for the models illustrated in Figs. 5 *B–E* and 6 *C* and *D* uses laser cut 0.75 mm thick PETG strips (1.1 cm in width) with holes for the vertex and scissor pivots. Scissor legs at vertex and scissor pivots are then joined with 4 mm brass eyelet rivets. However, we note that the revolute joints (rivets) used at vertex pivots do not exactly reproduce the kinematics of spherical vertex pivots

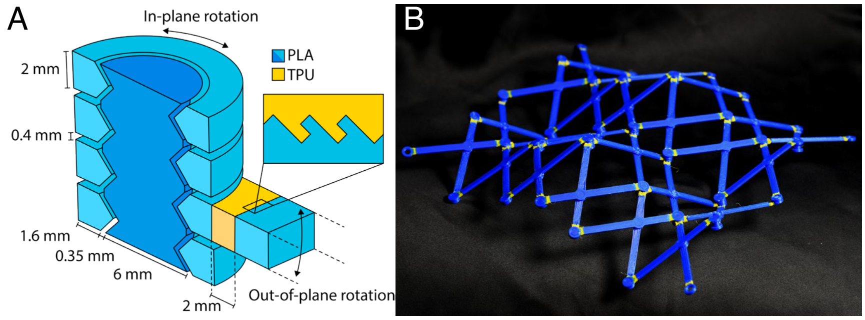

Fig. 7. 3D printed fabrication. (*A*) Schematic of the cross section of a single spherical vertex in 3D-printed fabrication. Rotational bearings enable in-plane rotation and TPU flexures enable out of plane rotation. Interlocked layers of TPU and PLA create a mechanical bond. (*B*) 3D printed eggbox model (compare to Fig. 6*C*).

as assumed in our mathematical treatment; in addition, this method requires individual assembly of each joint and as such is not suitable for rapid fabrication.

To address both limitations, we develop a multimaterial 3D printed fabrication which uses soft flexures to approximate the mechanics of spherical vertex pivots and allows for fully automated assembly (Fig. 7). We demonstrate our method by printing the eggbox model as a monolithic unit (all scissors and pivots are printed in place, with no additional assembly required). For further detail and comparison of fabrication methods see *SI Appendix*, section S.VI.

Numerical Simulation. To explore the mechanics and energetics of deployment we develop a bead-and-spring model to simulate pantograph lattices with both spherical and revolute vertex pivots, corresponding qualitatively to the two different types of fabrication we explored. Our simulations (*SI Appendix*, Figs. S20 and S21) suggest the possibility of engineering additional functionality into pantograph devices through control of deployment energetics and multistable deployed geometries. See *SI Appendix*, section S.VI for details.

Data, Materials, and Software Availability. Code data have been deposited in GitHub (https://github.com/Noahyt/PUBLIC-PANTOGRAPH-LATTICE).

ACKNOWLEDGMENTS. We thank the Harvard NSF MRSEC 20-11754, the Simons Foundation, and the Henri Seydoux Foundation for partial financial support. This work is partially supported by NSF Graduate Research Fellowship under Grant Nos. DGE 2140743, JSPS 24KJ0637, JST FOREST JPMJFR232T, and JST AdCORP JPMJKB2302.

1. S. J. P. Callens, A. A. Zadpoor, From flat sheets to curved geometries: Origami and kirigami approaches. *Mater. Today (Kidlington)* **21**, 241–264 (2018).
2. R. J. Lang, "A computational algorithm for origami design" in *Proceedings of the Twelfth Annual Symposium on Computational Geometry–SCG '96* (ACM Press, 1996), pp. 98–105.
3. L. Mahadevan, S. Rica, Self-organized origami. *Science* **307**, 1740 (2005).
4. L. H. Dudte, E. Vouga, T. Tachi, L. Mahadevan, Programming curvature using origami tessellations. *Nat. Mater.* **15**, 583–588 (2016).
5. G. P. T. Choi, L. H. Dudte, L. Mahadevan, Programming shape using kirigami tessellations. *Nat. Mater.* **18**, 999–1004 (2019).
6. L. H. Dudte, G. P. T. Choi, L. Mahadevan, An additive algorithm for origami design. *Proc. Natl. Acad. Sci. U.S.A.* **118**, e2019241118 (2021).
7. L. H. Dudte, G. P. T. Choi, K. P. Becker, L. Mahadevan, An additive framework for kirigami design. *Nat. Comput. Sci.* **3**, 443–454 (2023).
8. N. Toyonaga, L. Mahadevan, Structural dynamics of contractile injection systems. *Biophys. J.* **124**, 172–178 (2024).
9. S. Adriaenssens, P. Block, D. Veenendaal, C. Williams, *Shell Structures for Architecture: Form Finding and Optimization* (Routledge, ed. 1, 2014).
10. F. Maden, K. Korkmaz, Y. Akgün, A review of planar scissor structural mechanisms: Geometric principles and design methods. *Archit. Sci. Rev.* **54**, 246–257 (2011).
11. Z. You, S. Pellegrino, Foldable bar structures. *Int. J. Solids Struct.* **34**, 1825–1847 (1997).
12. C. Hoberman, "Reversibly expandable doubly-curved truss structure." US Patent 4942700A (1988).
13. S. Nishimoto, T. Tachi, Transformable surface mechanisms based on bending-active scissors structures. *J. IASS* **65**, 268–276 (2024).
14. D. Liu *et al.*, Deployable strip structures. *ACM Trans. Graph.* **42**, 1–16 (2023).
15. S. Pillwein, P. Musialski, Generalized deployable elastic geodesic grids. *ACM Trans. Graph.* **40**, 1–15 (2021).
16. G. C. Quinn, C. Gengnagel, "A review of elastic grid shells, their erection methods and the potential use of pneumatic formwork" in *4th International Conference on Mobile, Adaptable and Rapidly Assmbled Structures, MARAS2014* (2014), vol. 136.
17. J. Panetta, M. Konaković-Luković, F. Isvoranu, E. Bouleau, M. Pauly, X-shells: A new class of deployable beam structures. *ACM Trans. Graph.* **38**, 1–15 (2019).
18. Q. Becker *et al.*, C-shells: Deployable gridshells with curved beams. *ACM Trans. Graph.* **42**, 1–17 (2023).
19. C. Baek, A. O. Sageman-Furnas, M. K. Jawed, P. M. Reis, Form finding in elastic gridshells. *Proc. Natl. Acad. Sci. U.S.A.* **115**, 75–80 (2018).
20. A. O. Sageman-Furnas, A. Chern, M. Ben-Chen, A. Vaxman, Chebyshev nets from commuting PolyVector fields. *ACM Trans. Graph.* **38**, 1–16 (2019).
21. J. M. McCarthy, G. S. Soh, "Geometric design of linkages" in *Interdisciplinary Applied Mathematics*, S. S. Antman, J. E. Marsden, L. Sirovich, Eds. (Springer, ed. 2, 2010).
22. T. Tachi, Generalization of rigid-foldable quadrilateral-mesh origami. *J. Int. Assoc. Shell Spatial Struct.* **50**, 173–179 (2009).
23. F. Escrig, J. P. Valcarcel, Geometry of expandable space structures. *Int. J. Space Struct.* **8**, 71–84 (1993).
24. F. Ono, T. Tachi, "Growth deformation of surface with constant negative curvature by bending-active scissors structure" in *Proceedings of IASS Annual Symposia, 2022* (2022), pp. 1–12.
25. F. Ono *et al.*, Growth-induced transformable surfaces realized by bending-active scissors grid. *Archit. Intell.* **3**, 1–18 (2024).
26. N. Toyonaga, Pantograph Lattice. Github. https://github.com/Noahyt/PUBLIC-PANTOGRAPH-LATTICE. Deposited 10 Febuary 2025.